Single-Particle Cryo-EM and 3D Reconstruction of Hybrid Nanoparticles with Electron-Dense Components

*Guimei Yu, Rui Yan, Chuan Zhang, Chengde Mao, and Wen Jiang**

Single-particle cryo-electron microscopy (cryo-EM), accompanied with 3D reconstruction, is a broadly applicable tool for the structural characterization of macromolecules and nanoparticles. Recently, the cryo-EM field has pushed the limits of this technique to higher resolutions and samples of smaller molecular mass, however, some samples still present hurdles to this technique. Hybrid particles with electron-dense components, which have been studied using single-particle cryo-EM yet with limited success in 3D reconstruction due to the interference caused by electron-dense elements, constitute one group of such challenging samples. To process such hybrid particles, a masking method is developed in this work to adaptively remove pixels arising from electron-dense portions in individual projection images while maintaining maximal biomass signals for subsequent 2D alignment, 3D reconstruction, and iterative refinements. As demonstrated by the success in 3D reconstruction of an octahedron DNA/gold hybrid particle, which has been previously published without a 3D reconstruction, the devised strategy that combines adaptive masking and standard single-particle 3D reconstruction approach has overcome the hurdle of electron-dense elements interference, and is generally applicable to cryo-EM structural characterization of most, if not all, hybrid nanomaterials with electron-dense components.

1. Introduction

Single-particle cryo-electron microscopy (cryo-EM), with constant advancements to provide more and higher resolution structural information for a broader spectrum of samples,[1] is currently widely applied for structural characterization of macromolecules at subnanometer to near-atomic resolutions in biological science and related fields. In recent years, this technique has been further introduced to the nanotechnology-related researches to characterize in vitro synthesized nanoparticles.[2] In contrast to this broad applicability, there are also some types of samples that remain challenging to single-particle 3D reconstruction, such as samples of small molecular mass (i.e., <150 KDa for proteinous specimens).

Hybrid particles composed of biomass and electron-dense elements, including both natural and engineered particles,[3] constitute another group of samples that pose some challenges for single-particle 3D reconstruction. As such electron-dense components potentially interfere with the single-particle structural analysis causing biased or incorrect alignment of particles, 3D structural determination of such hybrid particles either was limited to low resolutions or completely failed.[3b,f–h] This was also the case for our recently published dataset of octahedral DNA nanocage encapsulating a gold nanoparticle,[4] which show well-maintained octahedron-like cages in the cryo-EM 2D images yet failed to be reconstructed in 3D with both our in house-developed program *jspr*[5] and other single-particle 3D reconstruction programs (e.g., RELION).[6]

G. Yu, R. Yan, Prof. W. Jiang
Markey Center for Structural Biology
Department of Biological Science
Purdue University
240 S Martin Jischke Dr, West Lafayette, IN 47907, USA
E-mail: jiang12@purdue.edu
Dr. C. Zhang, Prof. C. Mao
Department of Chemistry
Purdue University
560 Oval Drive, West Lafayette, IN 47907-2084, USA

DOI: 10.1002/smll.201500531

Motivated by this challenge of solving 3D structures of hybrid particles with electron-dense components, we devised and verified a single-particle 3D reconstruction strategy for these hybrid particles, in which pixels from electron-dense elements (referred to as "gold" pixels) were computationally removed and only the biomass signal was included in the particle orientation determination. At the end of iterative refinements with masked images without "gold" pixels, the final parameters of Euler angles and centers were applied to the corresponding original hybrid particles in generating the final 3D map. Specifically, we developed a new algorithm in a Python script "*maskGold.py*" (Script S1, Supporting Information), by which adaptive masks according to the distribution of such bright pixels in individual images were generated to remove electron-dense components with minimal loss of the biomass signals. The Otsu thresholding[7] and random walker segmentation[8] methods were applied to separate pixels of electron-dense components ("gold pixels") from those of biomass and background ("non-gold pixels"). The described 3D reconstruction strategy was first tested with simulated hybrid particles using our previously published, resolvable phage T7 datasets[9] and followed with tests on experimental hybrid particles, both of which worked successfully. In conclusion, we have devised a way to perform successful single-particle 3D reconstruction of hybrid particles with electron-dense element clusters, and as indicated by our test with simulated data, subnanometer or even better resolutions could potentially be achieved if the biomass structures of the hybrid particles are largely homogeneous.

2. Results and Discussion

2.1. The Increased "Gold" Intensities Made Single-Particle 3D Reconstruction More Challenging

To better understand the effects caused by the incoherent bright densities in 2D images, we used a small, previously published phage T7His capsid II particle dataset[9b] to simulate hybrid particles with central "gold" of different intensities, followed by single-particle 3D reconstruction analysis. Prior to adding the bright "gold" densities, each 2D image was first normalized by adjusting the mean value of background noise to 0 and sigma to 1. After such normalization, each pixel value reflects signal-to-noise ratio (SNR). As shown in **Figure 1**, hybrid particles with simulated central "gold" of different intensities were generated and processed independently using *jspr*[5] to evaluate their ability in giving correct initial models. As predicted, the interference of "gold" pixels with 2D alignment became more severe with the increase of "gold" pixel intensities; A "gold" core with intensity of 4 and higher above the icosahedral shell signal made the initial model building of phage T7 capsid II to fail (Figure 1). Such mimics of hybrid particles with central cores of different intensities, although largely simplified when compared to real hybrid particles in terms of potential variations of size, intensity, and position, CTF modulation, *etc*., confirmed that the presence of strong incoherent bright pixels in TEM images is problematic to single-particle cryo-EM 3D reconstruction.

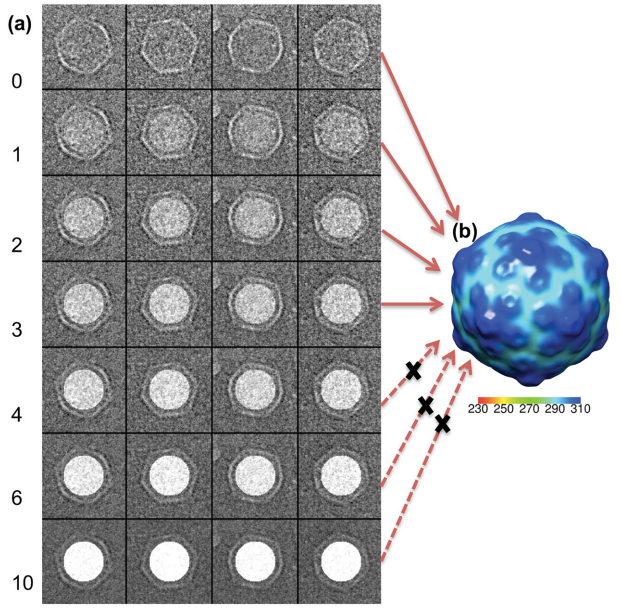

Figure 1. Simulated hybrid particles of phage T7His capsid II and "gold" cores with various intensities. (a) Simulated T7His CII/gold hybrid particles with "gold" of different intensities: "0," "1," "2," "3," "4," "6," and "10." (b) De novo initial model of phage T7His capsid II reconstructed from these simulated hybrid particles.

2.2. *maskGold.py*, an Adaptive Robust Masking Method

One natural way to address such hybrid particle 3D reconstruction challenge is to mask out all the bright pixels of "gold" yet preserve the coherent biomass signals in the 2D images for the alignments of particles during single-particle 3D reconstruction. To suffice this need, we developed a bright pixels masking algorithm, *maskGold.py*, based on Otsu thresholding[7] and random walker segmentation methods,[8] both of which are available in the *scikit-image* Python library[10] (see Methods). This image masking method has several attractive properties, including its robustness, sensitivity, and minimized loss of biomass signal. As shown in **Figure 2**a, simulated hybrid particles of T7His CII/"gold" with different central "gold" intensities were tested using *maskGold.py*. Accurate masks were robustly generated for all the hybrid particles containing central "gold" with intensities of 4–10. Proper masks could also be generated even for hybrid particles with central "gold" of intensity 3 that still gave correct 3D models in single-particle 3D reconstruction (Figure 1). Masks for some of the hybrid particles with central "gold" of intensity 2, however, did cover portions of CII pixels. Furthermore, we simulated T7His CII/"gold" hybrid particles with "gold" of different sizes, shapes, positions, and numbers, and tested with *maskGold.py*. Masks corresponding to the sizes, shapes, positions and numbers of simulated "gold" were generated precisely with minimum overlapping with non-gold pixels using the same set of parameter values of *maskGold.py* (Figure 2b). All these tests confirmed that *maskGold.py* could be a promising, robust masking method for a variety of hybrid particles with different metal cores, which accomplished the first step of 3D reconstruction of hybrid particles.

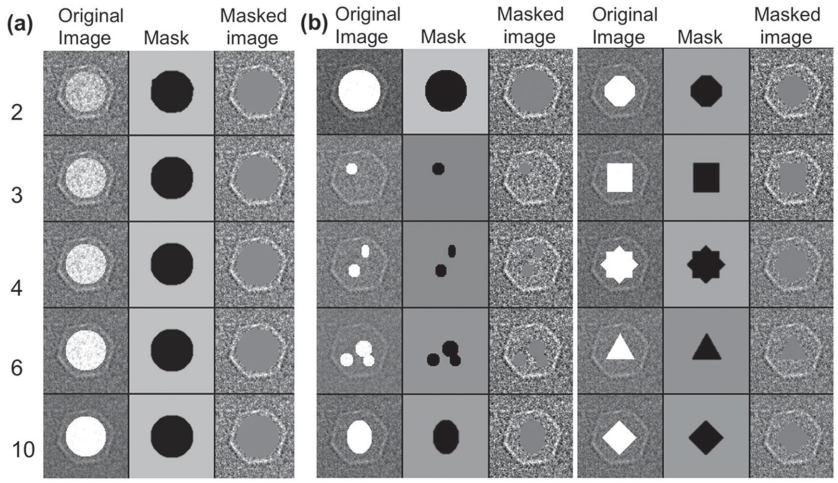

Figure 2. Adaptive masking of "gold" cores with different intensities, sizes, shapes, positions and amounts using *maskGold.py*. (a) Masking of T7His CII/"gold" hybrid particles containing "gold" of different intensities. (b) Masking of T7His CII/"gold" hybrid particles with "gold" of different sizes, amounts, positions, and shapes (all with an intensity of 10). "Original Image:" Input for *maskGold.py*. "Mask:" the mask generated by maskGold.py for "gold" pixels. "Masked Image:" Output of *maskGold.py*.

2.3. Successful 3D Reconstructions Were Achieved with Simulated Hybrid Particles after Masking with *maskGold.py*

Single-particle 3D reconstruction analysis was performed again for simulated phage T7His CII/"gold" hybrid particles after masking out "gold" pixels using *maskGold.py*. As expected, correct initial models were successfully obtained with the masked images (Figure S1, Supporting Information). To further test the possibility of using *maskGold.py*-processed particles for high-resolution single-particle 3D reconstruction, 5000 particles were randomly selected from another previously published, high-quality phage T7 MLD capsid II (MLDII) dataset that resulted in a 3.5 Å resolution structure.[9a] In order to better mimic the real situation, hybrid particles were simulated with variations of "gold" in shapes (circle to ellipse), sizes (140–180 pixels in diameter), positions (–4 to 4 pixels off center of box) and intensities (10–12); *maskGold.py* was used to mask out "gold" and generate masked images (**Figure 3**a). Single-particle 3D reconstructions were attempted for the simulated hybrid particles, particles with "gold" masked, and the corresponding original MLDII particles. Consistent with our aforementioned simulation shown in Figure 1, no correct initial models were obtained for the hybrid particles, while both the original and the masked particles gave correct, good-quality models (Figure 3b). Additionally, we found that even starting with a good initial model, the iterative refinement of the simulated hybrid particles readily drifted to wrong models after only one round of 2D alignment, regardless of the scoring functions used,

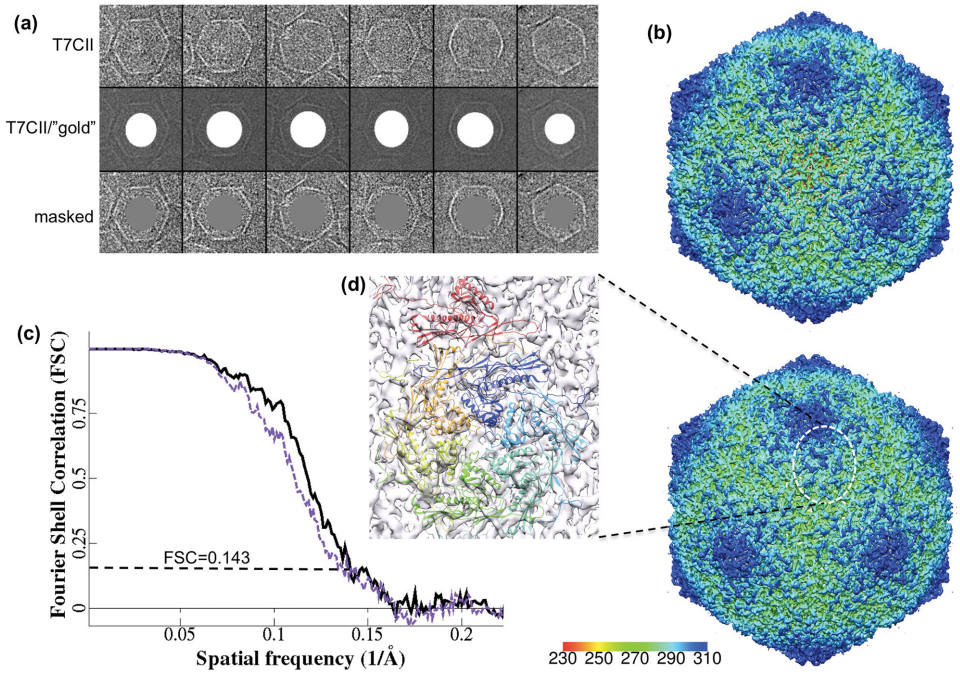

Figure 3. High resolution 3D reconstruction of simulated T7MLDII/"gold" particles. (a) Representative images of original T7MLDII particles, simulated hybrid particles, and particles with "gold" masked with *maskGold.py*. (b) 3D reconstructions of original T7MLDII (top) and *maskGold.py*-masked particles (bottom). (c) Fourier shell correlation curves for 3D reconstructions of original T7MLDII (black) and *maskGold.py*-masked particles (purple), which indicate resolutions of 7.1 Å (black) and 7.3 Å (purple), respectively, based on the 0.143 cutoff criterion. (d) Fitting of T7MLDII atomic structure (PDB ID: 3J7W) into an asymmetric unit in 3D map of *maskGold.py*-masked particles.

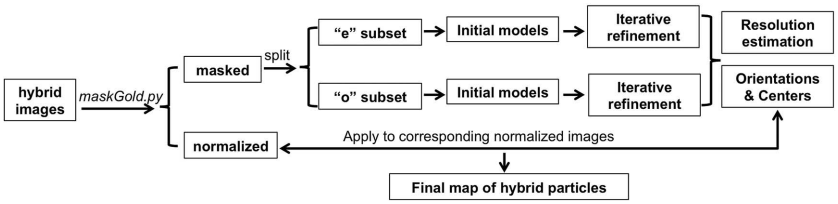

Figure 4. The flowchart of single particle 3D reconstruction of hybrid particles with electron-dense components.

such as cross-correlation coefficient (CCC), phase residual, Fourier ring coefficient (FRC),[11] and dot (Figure S2, Supporting Information). These results confirmed again that the presence of incoherent bright pixels in 2D images would cause problems in single-particle 3D reconstruction.

Iterative refinements with original particles and masked hybrid particles resulted in models of 7.1 Å and 7.3 Å resolutions, respectively (Figure 3c), from which the secondary structural elements (i.e., α-helix and β-sheet) of phage T7 capsid protein (gp10) were resolved (Figure 3d). The slightly worse quality of the map from masked images compared to the one from original images was understandable, considering the loss of "top" and "bottom" information of MLDII particles after masking. By applying the 2D alignment parameters (orientations and centers) of masked images (*.masked*) to the corresponding hybrid particles (*.norm*), a final 3D map for hybrid particles was generated with an icosahedral shell of virtually identical quality to the one from masked images (Figure S3, Supporting Information).

2.4. Single-Particle 3D Reconstruction Strategy for Hybrid Particles with Electron-Dense Components

After these tests with simulated T7/"gold" particles, we summarized a strategy for single-particle image processing of hybrid particles by combining *maskGold.py* masking with our truly independent single-particle 3D reconstruction method.[5] As illustrated in **Figure 4**, after preprocessing (i.e., particle picking and CTF parameters determination and correction), hybrid particles were first masked using *maskGold.py* resulting in two sets of particles, the normalized ones (*.norm*, with the non-gold pixels normalized to mean = 0 and sigma = 1) and the masked ones (*.masked*) derived from the normalized images (*.norm*) yet with gold pixels masked. The whole dataset of masked images was then split into two halves, "e" and "o" subsets, from which initial models and iterative refinements were performed independently. Resolution of the reconstruction was estimated based on the Fourier shell correlation between models from "e" and "o" subsets, and a final map of the hybrid particles could be obtained by pooling the two halves and applying the refinement parameters of masked particles (*.masked*) to the corresponding normalized particles (*.norm*). Although we have depicted this single-particle 3D reconstruction strategy of hybrid particles mainly based on our in-house-developed program *jspr*,[5] this strategy could be easily adapted to other single-particle 2D classification and 3D reconstruction programs.

2.5. *maskGold.py* Masking and Single-Particle 3D Reconstruction of Octahedron DNA/Gold Hybrid Particles

We revisited our previously published octahedral DNA/AuNP hybrid particle dataset[4] and processed this dataset using the image processing strategy described above (Figure 4). As shown in **Figure 5**a, cryo-EM images of this hybrid particle show a DNA shell wrapping around an AuNP close to the center of the shell. The average diameter of encapsulated AuNPs was around 5 nm with obvious size variation; therefore a regular fixed size mask for AuNPs in the images could not work optimally. Using *maskGold.py,* precise masks according to the size, shape, and position of AuNPs were generated to remove the bright pixels of AuNPs. A final reconstructed 3D map of 24 Å resolution was obtained (Figure 5b,c), which showed an octahedron cage with ≈14 nm long edges encapsulating a high-intensity sphere from averaged AuNPs. On each edge of the octahedron, there were two inward-protruding densities that could be attributed to the hybridized DNA strands linking the DNA nanocage with the encapsulated AuNP. Due to the size/position variations of encapsulated AuNPs as shown in Figure 5a, the DNA strand connections on AuNP surface were not observed in the reconstruction. Nevertheless, all other structural features shown in our reconstruction of octahedron DNA/AuNP hybrid particle agreed very well with the design (Figure 5d). In summary, the successful reconstruction of the octahedron DNA/AuNP hybrid particle with structural details matching initial design, demonstrated that our single-particle 3D reconstruction strategy is applicable to experimental hybrid particles with highly electron-dense, incoherent components.

2.6. *maskGold.py* Masking and Single-Particle 3D Reconstruction of Iron-Encapsulated Encapsulin Nanocompartment Hybrid Particles

We also tested our hybrid particle 3D reconstruction method on an iron-storage encapsulin nanocompartment that has recently been discovered and characterized.[3e] Four native encapsulin nanocompartment particles were extracted from a published figure[3e] and processed using our method. As shown in **Figure 6**a, pixels arising from encapsulated irons were masked successfully using *maskGold.py* with minimal over-masking of the encapsulin nanocompartment shells. Benefitting from the high symmetry (i.e., icosahedral), single-particle 3D reconstruction was successfully performed using only these four masked images (Figure 6a, masked image). A low-resolution (≈40 Å) 3D model was obtained (Figure 6b), which agreed well to the published encapsulin structure (EMDB-5953) that was reconstructed from purified iron core-free particles and low-pass filtered to similar resolution (Figure 6c). This test with iron-storage encapsulin further confirmed that our *maskGold.py* algorithm works well for both higher (e.g., Au) and lower (e.g., iron) intensity inorganic cores.

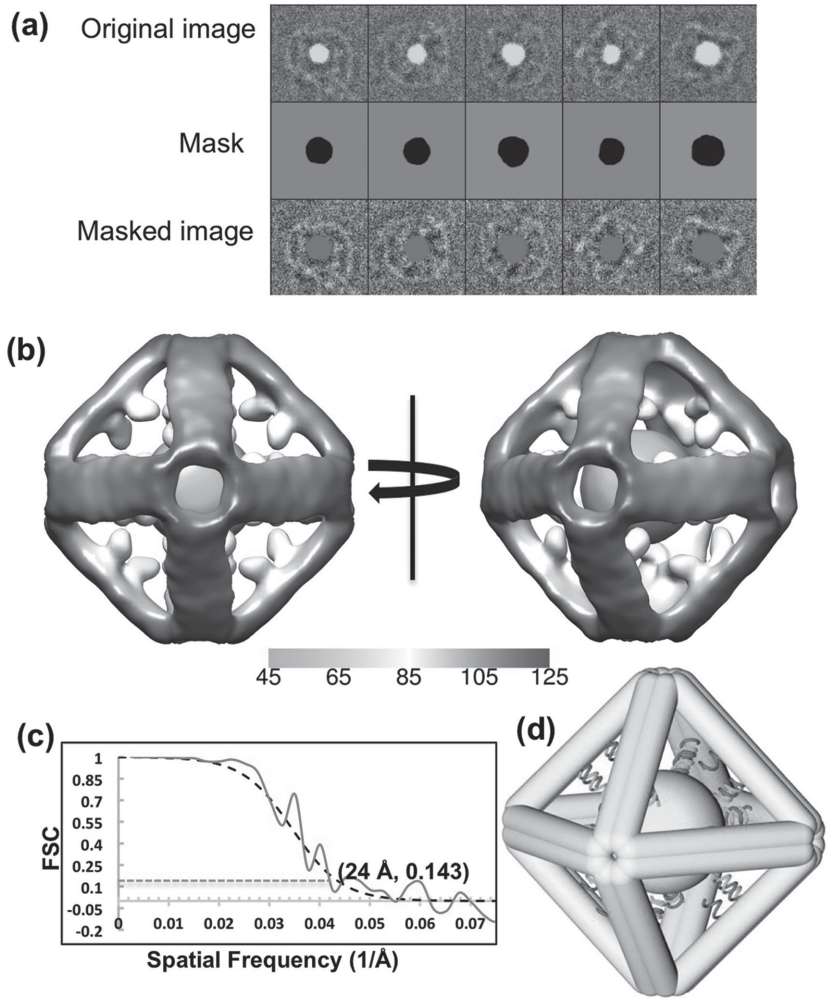

Figure 5. *MaskGold.py* masking and single particle 3D reconstruction of octahedral DNA/AuNP hybrid particles. (a) Representative cryo-EM images of octahedral DNA/AuNP hybrid particles, and their corresponding masks and masked images generated by *maskGold.py*. (b) 3D reconstruction of octahedral DNA/AuNP hybrid particles, with the map shown at two different views. (c) Fourier shell correlation curve. (d) The theoretical 3D model of octahedral DNA/AuNP hybrid particle based on initial design. Reproduced with permission.[4] Copyright 2015, American Chemical Society.

2.7. Discussion

Single-particle cryo-EM 3D reconstruction assumes that all the 2D images represent different projection views of a common 3D structure, and therefore, the homogeneity of samples is one of the most critical factors for achieving convergent 3D reconstruction. Another critical factor in single-particle 3D reconstruction is the low SNR of projection images due to low-dose imaging to minimize radiation damages to bioorganic structures. For most biological samples, noises mainly arise from electron scattering by buffer solutions and the grid substrate if continuous carbon is used. For the hybrid particles with electron-dense cores, however, the strong electron scattering by the heavy metal elements (e.g., Au) causes extra and much stronger incoherent signals superimposed on the coherent biomass signals (e.g., DNA cage). Since cryo-EM of typical biological samples is already severely limited by low SNR, such additional dominant interfering signals from heavy metal elements would erroneously bias the 2D alignment and make it challenging to obtain convergent 3D models of these hybrid particles.

In the present work, we have established a strategy for single-particle cryo-EM 3D reconstruction of hybrid particles with electron-dense components, in which a critical masking step was integrated into the standard procedure of single-particle 3D reconstruction. We have developed an adaptive "gold" pixels masking algorithm, *maskGold.py*, which as proven by our tests can mask out electron-dense components efficiently and accurately, regardless of the variations among particles. Importantly, using this single-particle 3D reconstruction strategy, we have successfully solved the structure of a previously unresolvable octahedral DNA/AuNP hybrid particle[4] to ≈24 Å using about 300 particles, which demonstrated the potential of using the devised 3D reconstruction strategy to characterize other DNA and/or protein nanocage/metal hybrid materials.

In order to test whether hybrid particles can be reconstructed to high resolutions (i.e., subnanometer), we used some previously published high quality phage T7 MLD capsid II images[9a] to simulate a hybrid particle dataset, from which we found that the simulated T7 MLD capsid II/"gold" hybrid particles could be reconstructed to a similar resolution (≈7.3 Å) as the original T7 MLD capsid II particles (≈7.1 Å) using our strategy. This indicates that although a portion of the top and bottom information of hybrid particle with electron-dense part(s) was lost, subnanometer or possibly even higher resolution 3D reconstructions of hybrid particles can potentially still be achieved.

A major remaining concern about the cryo-EM and 3D reconstruction technique when addressing experimental biomass/metal hybrid particle data was CTF estimation and correction, as the presence of metal elements might violate the weak phase object (WPO) assumption that the current CTF model is based on[12] and therefore cause improper correction of the CTF effect in TEM projection images. To evaluate the differences in CTF parameters between hybrid particles and biomass materials, we estimated the CTF parameters of several micrographs from the octahedral DNA/AuNP hybrid particle dataset[4] using empty areas without particles, hybrid particles, and shells alone (Au pixels masked), respectively; we found that the resulting CTF parameters, especially the most critical defocus values, were close among them, although the estimation of the noise levels show some differences (Figure S4,

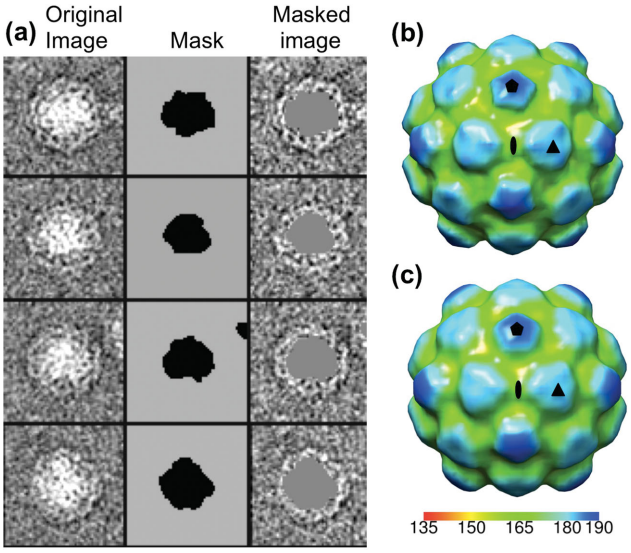

Figure 6. *MaskGold.py* masking of bright pixels from irons encapsulated inside encapsulin nanocompartments in cryo-EM images, and single particle 3D reconstruction. (a) "Original Image:" Four iron-encapsulated encapsulin nanocompartment particles extracted from Figure 2A in ref. [3e] (reproduced with permission.[3e] Copyright 2015, John Wiley and Sons); and the corresponding masks and masked images generated by *maskGold.py* processing. (b) 3D map reconstructed from the four masked particles in (a); (c) A 3D map of iron-free encapsulin nanocompartments (EMDB-5953) low-pass filtered to similar resolution as (b).

Supporting Information). This implied that the concern about electron-dense particles perturbing CTF determination and correction was probably not necessary when targeting at intermediate resolutions. However, more systematical studies are required to test whether it would be a problem for reaching higher resolutions.

3. Conclusion

We have developed and demonstrated a strategy for single-particle 3D reconstruction of hybrid particles with incoherent electron-dense element clusters, the presence of which has been shown problematic to single-particle 3D reconstruction technique and caused failed 3D reconstruction. This strategy can be easily adapted to most single-particle 3D reconstruction programs and can serve as a general methodology for single-particle cryo-EM structural characterization of most hybrid nanomaterials with coherent biomass frameworks yet with incoherent metal cores.

4. Experimental Section

Simulation of Hybrid Particles: A Python script, "*simGold.py*" (Script S2, Supporting Information), was developed based on the "skimage.draw" and "skimage.morphology" modules in scikit-image package,[10] and some functions from the EMAN2 library,[13] to simulate "gold" of different shapes, sizes, and positions, and generate hybrid particles. Multiple shapes including circle, ellipse, triangle, rectangle, octagon, diamond, and star have been included in the simulation. Initially, all pixels inside simulated shapes were set to pixel values of "1," while those outside were "0". By multiplying a specified number ("-marker_pixel" in *simGold.py*), we could vary the brightness of simulated "gold" cores. Original cryo-EM images were first normalized using the "*normalize.circlemean*" processor in EMAN2.[13] Briefly, an annulus of two pixels at a specified radius that was large enough to ensure no particle densities included, was used to estimate and normalize the background noise of each image to mean = 0, sigma = 1. The "gold" images were added to the normalized images to generate the hybrid particles.

Two experimental cryo-EM image sets were used to simulate hybrid particles. First, a previously published small dataset (258 particles) of phage T7His capsid II[9b] was used for simulation using *simGold.py* to evaluate and validate our proposed methods on selective masking and 3D reconstruction of hybrid particles. Second, a larger dataset of phage T710A MLD capsid II particles previously resolved to 3.5 Å resolution[9a] was used for demonstration of feasibility of high-resolution 3D reconstruction of hybrid particles. In this study, 5000 particles with a sampling rate of 2.2 Å per pixel were randomly selected from this dataset for hybrid particle simulation and high-resolution image processing. "Gold" particles with circle to ellipse shapes, diameters of 140–180 pixels, intensities of 10–12, and ±4 pixels center offsets were generated and applied to the normalized images of T7 MLDII using *simGold.py* as described above.

Masking of Electron-Dense Components from TEM Images Using MaskGold.py: Masking of the "gold" pixels from TEM images was performed using the *maskGold.py* algorithm that we developed using functions from EMAN2[13] and the numPy and scikit-image Python packages (Supplementary Script 1, Supporting Information). Images of hybrid particles were first rescaled to the pixel value range of –1 to 1, which will be the input to determine an optimal threshold for separating pixels from heavy ("gold" pixels) and light elements ("non-gold" pixels) and dividing them into two classes, "gold" and "non-gold." Otsu's thresholding method[7] was used to identify the optimal threshold (T_{Otsu}) that maximizes the inter-class variance while minimizing that of the intraclass. Due to noises, simple binary classification of the pixels based on this threshold will inevitably misassign both "gold" and "non-gold" pixels, often as scattered speckles in their respective regions. We thus further optimized the algorithm with an additional segmentation step that also takes consideration of spatial distribution of the pixels instead of only the pixel values. Pixels with values smaller than T_{Otsu}–0.5σ are assigned as seeds for "non-gold" regions, while pixels with values larger than T_{Otsu}+0.5σ are assigned as seeds for "gold" regions, and the rest pixels (between T_{Otsu}–0.5σ and T_{Otsu}+0.5σ) remain unassigned. Then, an anisotropic diffusion-based random walker segmentation algorithm[8] was used to adaptively grow both sets of seed pixels to generate contiguous image segments corresponding to the "gold" and "non-gold" regions, respectively. The segments were saved in mask image files compatible with EMAN2 and applied to mask the TEM images with the "non-gold" pixels normalized (mean = 0, sigma = 1). After *maskGold.py* processing, two image files will be generated, including a *.masked* file with "gold" masked that can be used for single-particle cryo-EM image processing, and a *.norm* file, which is normalized using only the "non-gold" pixels (mean = 0; sigma = 1) but keeping the "gold" region unmasked. Such normalization of hybrid particles in the *.norm* file, adjusted pixels of biomass in all

small NANO MICRO

the 2D images to a similar gray level without being disturbed by the variable "gold," which is essential for proper single-particle 3D reconstructions.[14] A final 3D model of both the "gold" and "non-gold" regions can be reconstructed in a single 3D map using the normalized, non-masked images (*.norm*) and the alignment parameters from corresponding masked images.

Single-Particle 3D Reconstruction Methods: Particles were selected using *e2boxer.py* in EMAN2.[13] Contrast transfer function (CTF) estimation was performed using *fitctf2.py*.[15] For hybrid particles with electron-dense components, bright pixels were masked out using *maskGold.py* as described above. Single-particle 3D reconstruction was mainly performed using the in-house-developed program *jspr* with truly independent reconstruction strategy, in which the masked images were split into two halves and processed independently.[5] Small subsets of particles were randomly chosen from individual half datasets, separately, assigned with random Euler angles and refined till convergence to obtain *de novo* initial models. Using the initial models as references, 2D alignment was performed using the "projection matching" method and 3D models were reconstructed with the "direct Fourier inversion" approach.[5] Fourier shell correlation (FSC) of 3D models from the two half datasets was calculated and the 0.143 cutoff was used to estimate the resolution of 3D reconstructions.[16]

DNA/AuNP Hybrid Particles: Cyro-EM images of octahedral DNA nanocage/gold nanoparticles (AuNPs) were used as the primary experimental hybrid particle dataset for testing the proposed methods in the present work. This dataset was previously published without a 3D reconstruction.[4] The digitized images were binned 4×4, resulting in a final sampling rate of 4.98 Å per pixel. The final 3D map has been deposited to the Electron Microscopy Data Bank with an accession code of 6367. More details on experimental generation of oct DNA/AuNP hybrid particles and cryo-EM imaging conditions can be found in the publication.[4]

Iron-Storage Encapsulin Nanocompartments: A recent study has reported the discovery and characterization of a new iron-storage encapsulin nanocompartment from *Myxiciccus xanthus*.[3e] A cryo-EM micrograph of this native encapsulin nanocompartment shown as Figure 2A in original publication[3e] was reused to test masking by *maskGold.py* with subsequent single-particle 3D reconstruction analysis.

Supporting Information

Supporting Information is available from the Wiley Online Library or from the author.

Acknowledgements

The authors thank Chris Benjamin, Frank Vago and Samir Parmar for help in the preparation of the manuscript. The authors thank ONR and NSF for supporting this work.

[1] a) X. C. Bai, I. S. Fernandez, G. McMullan, S. H. Scheres, *Elife* **2013**, *2*, e00461; b) W. Jiang, M. L. Baker, J. Jakana, P. R. Weigele, J. King, W. Chiu, *Nature* **2008**, *451*, 1130; c) W. Kuhlbrandt, *Science* **2014**, *343*, 1443; d) M. Liao, E. Cao, D. Julius, Y. Cheng, *Nature* **2013**, *504*, 107; e) H. Liu, L. Jin, S. B. Koh, I. Atanasov, S. Schein, L. Wu, Z. H. Zhou, *Science* **2010**, *329*, 1038; f) S. H. Scheres, *Elife* **2014**, *3*, e03665.

[2] a) X. C. Bai, T. G. Martin, S. H. W. Scheres, H. Dietz, *Proc. Natl. Acad. Sci. USA* **2012**, *109*, 20012; b) Y. He, T. Ye, M. Su, C. Zhang, A. E. Ribbe, W. Jiang, C. D. Mao, *Nature* **2008**, *452*, 198; c) T. Kato, R. P. Goodman, C. M. Erben, A. J. Turberfield, K. Namba, *Nano Lett.* **2009**, *9*, 2747; d) C. Zhang, M. Su, Y. He, X. Zhao, P. A. Fang, A. E. Ribbe, W. Jiang, C. D. Mao, *Proc. Natl. Acad. Sci. USA* **2008**, *105*, 10665.

[3] a) J. Boskovic, A. Rivera-Calzada, J. D. Maman, P. Chacon, K. R. Willison, L. H. Pearl, O. Llorca, *EMBO J.* **2003**, *22*, 5875; b) C. Chen, M. C. Daniel, Z. T. Quinkert, M. De, B. Stein, V. D. Bowman, P. R. Chipman, V. M. Rotello, C. C. Kao, B. Dragnea, *Nano Lett.* **2006**, *6*, 611; c) S. K. Dixit, N. L. Goicochea, M. C. Daniel, A. Murali, L. Bronstein, M. De, B. Stein, V. M. Rotello, C. C. Kao, B. Dragnea, *Nano Lett.* **2006**, *6*, 1993; d) P. K. Lo, P. Karam, F. A. Aldaye, C. K. McLaughlin, G. D. Hamblin, G. Cosa, H. F. Sleiman, *Nat. Chem.* **2010**, *2*, 319; e) C. A. McHugh, J. Fontana, D. Nemecek, N. Q. Cheng, A. A. Aksyuk, J. B. Heymann, D. C. Winkler, A. S. Lam, J. S. Wall, A. C. Steven, E. Hoiczyk, *EMBO J.* **2014**, *33*, 1896; f) L. Montesano-Roditis, D. G. Glitz, R. R. Traut, P. L. Stewart, *J. Biol. Chem.* **2001**, *276*, 14117; g) J. Sun, C. DuFort, M. C. Daniel, A. Murali, C. Chen, K. Gopinath, B. Stein, M. De, V. M. Rotello, A. Holzenburg, C. C. Kao, B. Dragnea, *Proc. Natl. Acad. Sci. USA* **2007**, *104*, 1354; h) Z. Zhao, E. L. Jacovetty, Y. Liu, H. Yan, *Angew. Chem. Int. Ed. Engl.* **2011**, *50*, 2041; i) T. Zhou, Y. J. Wang, Y. C. Dong, C. Chen, D. S. Liu, Z. Q. Yang, *Bioorgan. Med. Chem.* **2014**, *22*, 4391.

[4] C. Zhang, X. Li, C. Tian, G. M. Yu, Y. L. Li, W. Jiang, C. D. Mao, *ACS Nano* **2014**, *8*, 1130.

[5] F. Guo, W. Jiang, *Methods Mol. Biol.* **2014**, *1117*, 401.

[6] S. H. Scheres, *J. Struct. Biol.* **2012**, *180*, 519.

[7] N. Otsu, *IEEE Trans. Syst. Man Cybernetics* **1979**, *9*, 62.

[8] L. Grady, *IEEE Trans. Pattern Anal.* **2006**, *28*, 1768.

[9] a) F. Guo, Z. Liu, P. A. Fang, Q. F. Zhang, E. T. Wright, W. M. Wu, C. Zhang, F. Vago, Y. Ren, J. Jakana, W. Chiu, P. Serwer, W. Jiang, *Proc. Natl. Acad. Sci. USA* **2014**, *111*, E4606; b) G. Yu, F. Vago, D. Zhang, J. E. Snyder, R. Yan, C. Zhang, C. Benjamin, X. Jiang, R. J. Kuhn, P. Serwer, D. H. Thompson, W. Jiang, *J. Struct. Biol.* **2014**, *187*, 1.

[10] S. van der Walt, J. L. Schonberger, J. Nunez-Iglesias, F. Boulogne, J. D. Warner, N. Yager, E. Gouillart, T. Yu, *PeerJ* **2014**, *2*, e453.

[11] M. Vanheel, *Ultramicroscopy* **1987**, *21*, 95.

[12] C. Yang, W. Jiang, D. H. Chen, U. Adiga, E. G. Ng, W. Chiu, *J. Microsc. Oxford* **2009**, *233*, 391.

[13] G. Tang, L. Peng, P. R. Baldwin, D. S. Mann, W. Jiang, I. Rees, S. J. Ludtke, *J. Struct. Biol.* **2007**, *157*, 38.

[14] C. O. Sorzano, L. G. de la Fraga, R. Clackdoyle, J. M. Carazo, *Ultramicroscopy* **2004**, *101*, 129.

[15] W. Jiang, F. Guo, Z. Liu, *J. Struct. Biol.* **2012**, *180*, 343.

[16] a) P. B. Rosenthal, R. Henderson, *J. Mol. Biol.* **2003**, *333*, 721; b) S. H. Scheres, S. Chen, *Nat. Methods* **2012**, *9*, 853.

Received: February 23, 2015
Revised: June 13, 2015
Published online: July 14, 2015

